Journal of Solid Mechanics Vol. 16, No. 3 (2024) pp. 288-313
DOI: 10.60664/jsm.2024.0091642

Research Paper

Vibration Study on Multilayer Sandwich Plates: Porous FGM Core, Nanocomposite and Piezoelectric Face Sheets

M. Pakize [1], M. Irani Rahaghi [2], Z. Khoddami Maraghi [2], S. Niknejad [3], A. Ghorbanpour Arani [1,3*]

[1] *Department of Solid Mechanics, Faculty of Mechanical Engineering, University of Kashan, Kashan, Iran*
[2] *Faculty of Engineering, Mahallat Institute of Higher Education, Mahallat, Iran*
[3] *Institute of Nanoscience & Nanotechnology, University of Kashan, Kashan, Iran*

Received 13 September 2020; Received in revised form 28 April 2021; Accepted 26 October 2022

ABSTRACT

A quasi-3D sinusoidal shear deformation theory and an analytical solution are presented for free vibration analysis of a 5-layer sandwich plate. The core of the sandwich plate is composed of a functionally graded porous (FGP) material that is distributed in two different types of nonlinear functions. The porous core is surrounded by two randomly oriented straight single walled CNT reinforced layers and two piezoelectric face sheets. Eight various couples of distribution of CNTs are considered for interior layers of the sandwich plate. Symmetric distributions include uniform distribution and FG-XX, FG-OO, and FG-VA and asymmetric distributions are FG-XO, FG-UO, FG-UX, and FG-AV. Effective elastic moduli of the nanocomposite layers are calculated by Mori-Tanaka approach; the set of the governing equations are derived using Hamilton's principle and are solved for the simply supported boundary conditions using Navier's method. Accuracy of the presented solution is confirmed and effects of different parameters on the natural frequencies of the plate are studied including aspect ratio, porosity parameter, porosity distribution pattern, volume fraction and distribution pattern of CNTs and Winkler and shear coefficients of the foundation.

Keywords: Vibration; Sandwich plate; Quasi-3D plate theory; Porous; Carbon nanotube.

*Corresponding author. Tel.: +98 31 55912450, Fax: +98 31 55912424.
E-mail address: aghorban@kashanu.ac.ir

1 INTRODUCTION

DUE to their excellent multi-functionality offered by low specific weight, the efficient capacity of energy dissipation and enhanced recyclability, porous materials are receiving worldwide interests as advanced engineering materials in mechanical, aerospace and civil engineering. There are a considerable number of papers regarding the mechanical analysis of FGP structures. Chen et al. [1] studied static bending and mechanical buckling analyses of shear deformable FGP beams. They focused on the influences of the porosity parameter and slenderness ratio of the beam on the bending and buckling characteristics of FGP beams. In another study, they studied free and forced vibration analysis of FGP beams [2]. They presented a parametric study to examine the influences of porosity parameter, porosity distribution pattern, slenderness ratio and boundary condition on the natural frequencies and dynamic response of FGP beams. In another work, They investigated nonlinear free vibration analysis of sandwich beams with an FGP core [3]. This time, they presented a parametric study to examine the influences of porosity parameter, slenderness ratio and thickness ratio on the linear and nonlinear natural frequencies. Size-dependent nonlinear vibration analysis of FGP tapered microbeams was investigated by Shafiei et al. [4]. They studied the effects of amplitude, material length scale, rate of thickness and porosity parameter on the nonlinear fundamental frequency of FGP tapered microbeams. Ebrahimi and Jafari [5] focused on the thermo-mechanical vibration characteristic of FGP beams in a thermal environment. They investigated the influences of porosity parameter, porosity distribution pattern, thermal load, boundary conditions and power-low exponent on the natural frequencies of FGP beams. Using a refined four-variable plate theory, Barati and Zenkour [6] studied electro-thermo-mechanical vibrational analysis of FGP piezoelectric plates. They discussed the effects of porosity distribution pattern, applied voltage, thermal load, material gradation, geometrical parameters and boundary conditions on the natural frequencies of FGP plates. Ebrahimi and Barati [7] studied size-dependent and porosity-dependent vibration analysis of magneto-electro-elastic FGP nanobeams resting on a two-parameter elastic foundation. They presented some numerical results to show the effects of porosity parameter, elastic and shear coefficients of foundation, magnetic potential, applied voltage, scale coefficient, material gradation and slenderness ratio on the natural frequencies of FGP nanobeams. Free vibration analysis of CNT-reinforced cylindrical shells made of FGP materials with temperature-dependent properties under thermal load was investigated by Safarpour et al. [8]. They presented a parametric study to show the influences of length to radius ratio, porosity parameter, thermal load and boundary conditions on the natural frequency of FGP cylindrical shells. Using a quasi-3D hyperbolic shear deformation plate theory, Shahsavari et al. [9] studied free vibration behavior of FGP plates resting on elastic foundations. They presented comprehensive parametric results to study the influences of volume fraction index, porosity fraction index and geometrical parameters on the natural frequencies of FGP plates. Daikh and Zenkour [10] proposed a new porosity for bending analysis of various functionally graded sandwich plates. They used a New higher-order deformation theory to derive the field equations of the FG sandwich plate. Numerical results presented to show the effect of the material distribution, the sandwich plate geometry and the porosity on the deflections and stresses of FG sandwich plates. A quasi-3D tangential shear deformation theory was employed by Amir et al. [11] to analyze the free vibration behavior of a three-layered FG porous micro plate integrated by nanocomposite faces in a hygrothermal environment that rested on Pasternak foundation. They used Hamilton's principle and Navier's solution to extract and solve motion equations, respectively. Akbari et al. [12] presented a numerical solution for free vibration analysis of sandwich cylindrical panels made of a saturated FGP core and two similar homogenous face sheets. They focused on the influence of various parameters on the natural frequencies such as geometrical parameters of the panel, porosity parameter, porosity distribution pattern, thickness ratio and compressibility of pore fluid.

Due to their extraordinary mechanical, thermal and electrical properties, CNTs can be used as reinforcements of polymer composites. So, since the discovery of CNTs in 1991 by Ijima [13], many researchers have focused on mechanical analysis of FG-CNTRC structures. Ghorbanpour Arani et al. [14] used an analytical approach as well as the finite element method (FEM) and studied buckling analysis of CNT-reinforced laminated composite plates. They focused on the influences of the orientation angle of CNTs, boundary conditions and the aspect ratio on the critical buckling load. Wang and Shen [15] studied nonlinear bending and vibration analyses of sandwich plates with CNT-reinforced composite face sheets resting on an elastic foundation in thermal environments. They presented a parametric study to show the influences of volume fraction of CNTs, core-to-face sheet thickness ratio, temperature elevation and foundation stiffness on the nonlinear bending and vibration characteristics. Using FEM, Zhu et al. [16] presented numerical solutions for bending and free vibration analyses of CNT-reinforced composite plates. They focused on the effects of boundary conditions, the volume fraction of CNTs and the edge-to-thickness ratios on the bending responses, natural frequencies and mode shapes of the plate. Lei et al. [17, 18] used element-free kp-Ritz method and presented numerical solutions for buckling and free vibration analyses of FG CNT-reinforced composite

plates. They devoted their results to examine the influences of volume fraction of CNTs, plate width-to-thickness ratio, plate aspect ratio, loading condition and temperature on the critical buckling load and natural frequencies. Bhardwaj et al. [19] studied non-linear dynamic response of CNT-reinforced laminated composite plates. They focused on the effects of volume fraction of CNTs and the aspect ratio of the plate on the non-linear dynamic deflection of laminated composite plates. Based on the three-dimensional theory of elasticity, Alibeigloo [20] investigated bending analysis of FG CNT-reinforced simply supported composite plates embedded in thin piezoelectric layers. He studied the influences of volume fraction and distribution pattern of CNTs, the thickness of piezoelectric layers and length to thickness ratio on the static behavior of the hybrid plate. Using FEM, static bending analysis of FG CNT-reinforced composite plates subjected to non-uniform elevated temperature fields was investigated by Jeyaraj and Rajkumar [21]. They studied the effects of boundary conditions, the distribution pattern of CNTs and type of thermal loading on the static characteristics of the plate. Using a QUAD-8 shear flexible element developed based on higher-order structural theory, Natarajan et al. [22] investigated bending and free vibration analysis of sandwich plates with CNT-reinforced face sheets. The presented a parametric study to examine the effects of volume fraction of CNTs, and core-to-face sheet thickness on the bending and free vibration characteristics of the sandwich plate. Wattanasakulpong and Chaikittiratana [23] studied static bending and free vibration analyses of CNT-reinforced composite plates resting on the Pasternak foundation. They focused on the effects of volume fraction of CNTs, elastic and shear characteristics of the foundation and geometrical parameters of the plate on the static bending and free vibration characteristics of the plate. Free and forced vibration analysis of viscoelastic micro composite beams reinforced by FG CNTs was studied analytically by Mohammadimehr et al. [24]. They presented some parametric results to examine the influences of volume fraction and distribution of CNTs and also damping coefficients on the natural frequencies and dynamic response of microcomposite beams. In another work on the micro-magneto-electro-elastic sandwich panel with a transversely flexible core and functionally graded carbon nanotube–reinforced nanocomposite facesheets, Mohammadimehr et al. [25], studied free vibration analysis of this structure based on high-order sandwich panel theory and modified strain gradient theory. They focused on the influences of the volume fraction, the various distributions of carbon nanotubes, the multi-physical fields, open- and closed-circuit boundary conditions, the material length scale parameters, different face sheet and core thicknesses, and temperature changes on the natural frequency. Their obtained results can be used to prevent the resonance phenomenon.

Ghorbanpour Arani et al. [26, 27] presented numerical solutions for free and forced vibration and supersonic flutter analyses of laminated FG-CNT reinforced cylindrical panels subjected to supersonic yawed flow. They presented parametric results to examine the influences of volume fraction, distribution pattern and orientation of CNTs, yaw angle and geometrical parameters of the panel on the natural frequencies and critical velocity of the panel. Arefi et al. [28] by using the modified couple stress theory as a non-classical continuum method and first-order shear deformation theory, studied the free vibration analysis of elastic three-layered nano-/micro-plate with exponentially graded core and piezomagnetic face sheets. They applied Navier's solution as an analytical solution to solve seven governing equations of motion.

In the presented paper, an exact solution is presented for free vibration analysis of a 5-layer simply supported sandwich plate consisted of an FGP core, CNT-reinforced interior layers and piezoelectric face sheets resting on Winkler/Pasternak foundation. The porosity of the core is evenly and unevenly repartitioned through the thickness. For its simplicity and accuracy even at a high volume fraction of inclusions, Mori-Tanaka approach is utilized to estimate the effective moduli of the nanocomposite layers. Accuracy of the presented analysis is confirmed and the influences of various parameters on the natural frequencies of the plate are investigated such as aspect ratio, porosity parameter and distribution pattern of pores, volume fraction and distribution pattern of CNTs and also Winkler and shear coefficients of the foundation.

2 PROBLEM DESCRIPTION AND THE GOVERNING EQUATIONS

As depicted in Fig. 1, a sandwich rectangular plate of total thickness h and dimensions a×b resting on an elastic foundation is considered. As Fig. 1 shows, the plate is made of an FG-porous core of thickness h_c, two FG-CNT reinforced interior layers of thickness h_{nc} and two piezoelectric face sheets of thickness h_p. As we're using the energy method to drive equations, the total potential energy of the structure should be determined. Considering the stress-strain relation of each layer and using quasi-3D sinusoidal theory, strain and kinetic energy of the porous, nanocomposite and piezoelectric layers are calculated separately.

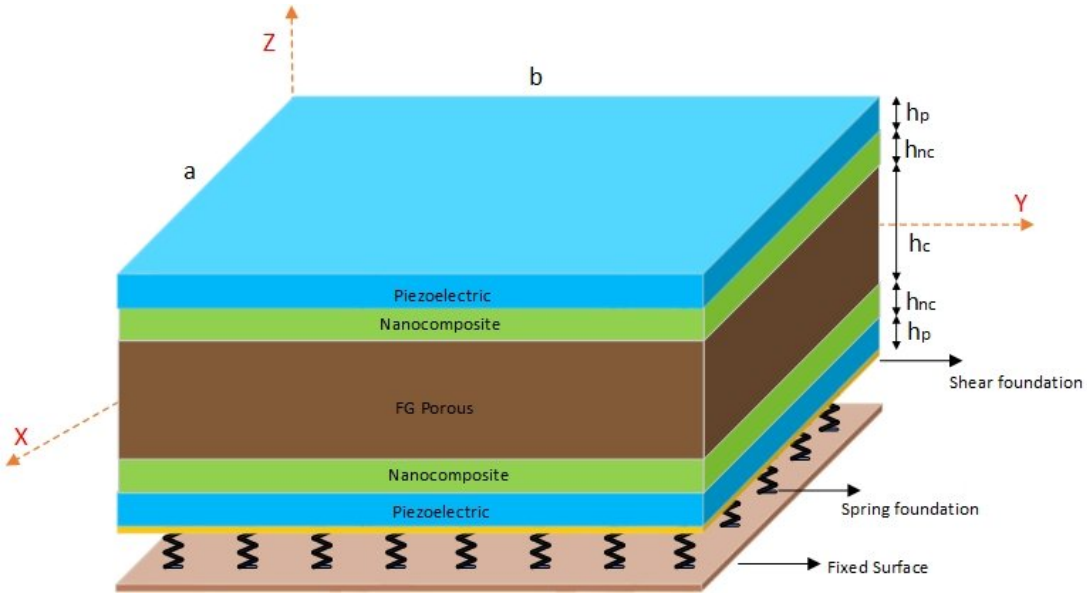

Fig. 1
Effect of step location on first two natural frequencies (Clamp boundary conditions) ($\tau = 0.75, k = 10^5 Nm^{-2}$).

2.1 Displacement field

The specified displacement field for this structure is a quasi-3D sinusoidal theory proposed by Zenkour [29,30] in which the stress-free boundary conditions on the top and bottom surfaces of the plate is applied [30]. Using sinusoidal functions first proposed by Levy [31] and assessed by Stein [32]. Simplicity and accuracy of these functions and the fact that they consider both normal and shear deformations caused Zenkour to use and develop them. Based on the quasi-3D sinusoidal shear deformation theory, components of displacement in a rectangular plate can be considered as [29]

$$u_1(x,y,z,t) = u(x,y,t) - z\frac{\partial w(x,y,t)}{\partial x} + f(z)\varphi_x(x,y,t)$$

$$u_2(x,y,z,t) = v(x,y,t) - z\frac{\partial w(x,y,t)}{\partial y} + f(z)\varphi_y(x,y,t) \quad (1)$$

$$u_3(x,y,z,t) = w(x,y,t) + \frac{df(z)}{dz}\varphi_z(x,y,t)$$

where u_1, u_2 and u_3 are displacement in x, y and z directions respectively and u, v and w show corresponding components of displacement at the middle surface of the plate (z=0). φ_x and φ_y stand for rotations around y and x axes, respectively, φ_z is an unknown function and f(z) is defined as following [33, 34]:

$$f(z) = \frac{h}{\pi}\sin\left(\frac{\pi z}{h}\right) \quad (2)$$

Based on the strain-displacement relations in x-y-z coordinates, components of the strain can be calculated using Eq. (1) as [35]

$$\varepsilon_{xx}=\frac{\partial u_1}{\partial x}=\frac{\partial u}{\partial x}-z\frac{\partial^2 w}{\partial x^2}+f\left(z\right)\frac{\partial \varphi_x}{\partial x}$$

$$\varepsilon_{yy}=\frac{\partial u_2}{\partial y}=\frac{\partial v}{\partial y}-z\frac{\partial^2 w}{\partial y^2}+f\left(z\right)\frac{\partial \varphi_y}{\partial y}$$

$$\varepsilon_{zz}=\frac{\partial u_3}{\partial z}=\frac{d^2 f}{dz^2}\varphi_z$$

$$\gamma_{yz}=\frac{\partial u_2}{\partial z}+\frac{\partial u_3}{\partial y}=\frac{df\left(z\right)}{dz}\left(\varphi_y+\frac{\partial \varphi_z}{\partial y}\right) \tag{3}$$

$$\gamma_{xz}=\frac{\partial u_1}{\partial z}+\frac{\partial u_3}{\partial x}=\frac{df\left(z\right)}{dz}\left(\varphi_x+\frac{\partial \varphi_z}{\partial x}\right)$$

$$\gamma_{xy}=\frac{\partial u_1}{\partial y}+\frac{\partial u_2}{\partial x}=\frac{\partial u}{\partial y}+\frac{\partial v}{\partial x}+f\left(z\right)\left(\frac{\partial \varphi_x}{\partial y}+\frac{\partial \varphi_y}{\partial x}\right)-2z\frac{\partial^2 w}{\partial x\partial y}$$

2.2 Porous core

A pore is a void space in a solid structure. A material that contains pores is called porous. Porosity is a fraction of the volume of pores over the total volume. It varies from 0% to 100%. The relation between stress and strain tensors can be specified using Hook's law. For the porous core following relation can be considered [36]:

$$\begin{Bmatrix}\sigma_{xx}\\ \sigma_{yy}\\ \sigma_{zz}\\ \tau_{yz}\\ \tau_{xz}\\ \tau_{xy}\end{Bmatrix}=\begin{bmatrix}C_{11} & C_{12} & C_{13} & 0 & 0 & 0\\ C_{21} & C_{22} & C_{23} & 0 & 0 & 0\\ C_{31} & C_{32} & C_{33} & 0 & 0 & 0\\ 0 & 0 & 0 & C_{44} & 0 & 0\\ 0 & 0 & 0 & 0 & C_{55} & 0\\ 0 & 0 & 0 & 0 & 0 & C_{66}\end{bmatrix}\begin{Bmatrix}\varepsilon_{xx}\\ \varepsilon_{yy}\\ \varepsilon_{yy}\\ \gamma_{yz}\\ \gamma_{xz}\\ \gamma_{xy}\end{Bmatrix} \tag{4}$$

in which $\gamma_{ij}=2\varepsilon_{ij}$ indicates to shear strain and

$$C_{11}=C_{22}=C_{33}=\frac{\left(1-\nu_c\right)E_c}{(1+\nu_c)(1-2\nu_c)}$$

$$C_{12}=C_{21}=C_{13}=C_{31}=C_{23}=C_{32}=\frac{\nu_c E_c}{(1+\nu_c)(1-2\nu_c)} \tag{5}$$

$$C_{44}=C_{55}=C_{66}=G_c=\frac{E_c}{2\left(1+\nu_c\right)}$$

where E_c, G_c and υ_c are elasticity modulus, shear modulus and Poisson's ratio of the porous core respectively. In this paper, two patterns are considered for the distribution of pores which are depicted in Fig. 2. For this cases elasticity modulus, shear modulus and density (ρ_c) are defined as [37,38]
Even porosity:

$$E_c(z)=E_1\left[1-e_1\cos\left(\frac{\pi z}{h_c}\right)\right]$$
$$G_c(z)=G_1\left[1-e_1\cos\left(\frac{\pi z}{h_c}\right)\right] \tag{6}$$
$$\rho_c(z)=\rho_1\left[1-e_m\cos\left(\frac{\pi z}{h_c}\right)\right]$$

Uneven porosity:

$$E_c(z)=E_1\left[1-e_1\cos\left(\frac{\pi z}{2h_c}+\frac{\pi}{4}\right)\right]$$
$$G_c(z)=G_1\left[1-e_1\cos\left(\frac{\pi z}{2h_c}+\frac{\pi}{4}\right)\right] \tag{7}$$
$$\rho_c(z)=\rho_1\left[1-e_m\cos\left(\frac{\pi z}{2h_c}+\frac{\pi}{4}\right)\right]$$

where E_1, G_1 and ρ_1 are specified in Fig. 2, $0\le e_1<1$ is porosity parameter which shows the size of pores and

$$e_m=1-\sqrt{1-e_1} \tag{8}$$

It is worth mentioning that in porous materials Poisson's ratio can be considered as a constant value.

2.3 CNT-reinforced layers

As depicted in Fig. 1. The porous core is surrounded by two CNT-reinforced layers. The CNTs are distributed uniformly with randomly orientated directions. According to the rule of mixture, the density of a CNT-reinforced polymer can be calculated as follow:

$$\rho=\rho_m V_m+\rho_r V_r, \tag{9}$$

in which ρ and V indicate density and volume fraction respectively and subscripts m and r indicate polymer matrix and CNT reinforcement, respectively.

In this paper, five linear types of CNTs distribution patterns are considered. The volume fraction of CNTs for these patterns can be stated as

Upper layer ($0.5h_c\le z\le 0.5h_c+h_{nc}$):

$$V_r(z)=\begin{cases} V_r^* & U \\ \left[1+\dfrac{2}{h_{nc}}\left(z-\dfrac{h_c+h_{nc}}{2}\right)\right]V_r^* & FG-V \\ \left[1-\dfrac{2}{h_{nc}}\left(z-\dfrac{h_c+h_{nc}}{2}\right)\right]V_r^* & FG-A \\ \dfrac{4}{h_{nc}}\left|z-\dfrac{h_c+h_{nc}}{2}\right|V_r^* & FG-X \\ 2\left(1-\dfrac{2}{h_{nc}}\left|z-\dfrac{h_c+h_{nc}}{2}\right|\right)V_r^* & FG-O \end{cases} \tag{10}$$

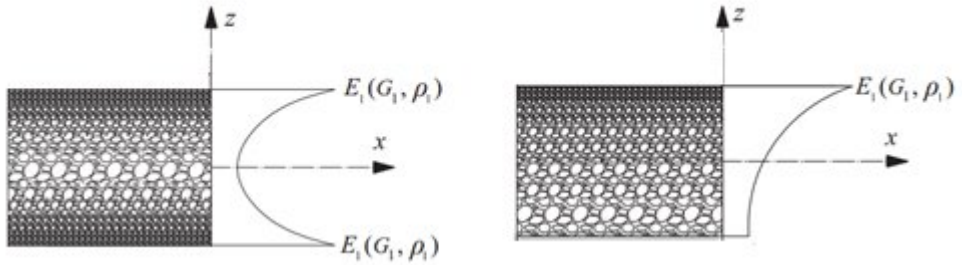

Fig. 2
Distribution patterns of pores.

Lower layer ($-0.5h_c-h_{nc} \leq z \leq -0.5h_c$):

$$V_r(z) = \begin{cases} V_r^* & U \\ \left[1+\dfrac{2}{h_{nc}}\left(z+\dfrac{h_c+h_{nc}}{2}\right)\right]V_r^* & FG-V \\ \left[1-\dfrac{2}{h_{nc}}\left(z+\dfrac{h_c+h_{nc}}{2}\right)\right]V_r^* & FG-A \\ \dfrac{4}{h_{nc}}\left|z+\dfrac{h_c+h_{nc}}{2}\right|V_r^* & FG-X \\ 2\left(1-\dfrac{2}{h_{nc}}\left|z+\dfrac{h_c+h_{nc}}{2}\right|\right)V_r^* & FG-O \end{cases}. \tag{11}$$

Also, the volume fraction of the polymer matrix can be obtained using the following relation:

$$V_m = 1 - V_r. \tag{12}$$

In Eqs. (10) and (11), V^*_r is the total mass fraction of CNTs which can be calculated based on the mass fraction of CNTs (w_r) as follow:

$$V_r^* = \left[1+\frac{\rho_r}{\rho_m}\left(\frac{1}{w_r}-1\right)\right]^{-1} \tag{13}$$

As the CNTs are orientated randomly, the CNT-reinforced matrix can be considered as an isotropic structure and Eq. (4) can be used for CNT-reinforced layers as well, in which

$$\begin{aligned} C_{11} &= C_{22} = C_{33} = \frac{(1-\nu_{nc})E_{nc}}{(1+\nu_{nc})(1-2\nu_{nc})} \\ C_{12} &= C_{21} = C_{13} = C_{31} = C_{23} = C_{32} = \frac{\nu_{nc}E_{nc}}{(1+\nu_{nc})(1-2\nu_{nc})} \\ C_{44} &= C_{55} = C_{66} = G_{nc} = \frac{E_{nc}}{2(1+\nu_{nc})} \end{aligned} \tag{14}$$

where elastic modulus (E_{nc}) and Poisson's ratio (ν_{nc}) of the CNT-reinforced layers can be estimated using the Eshelby–Mori–Tanaka scheme as

$$E_{nc}=\frac{9K_{nc}G_{nc}}{3K_{nc}+G_{nc}},\quad \nu_{nc}=\frac{3K_{nc}-2G_{nc}}{6K_{nc}+2G_{nc}}, \tag{15}$$

in which G_{nc} and K_{nc} are shear and bulk moduli of the CNT-reinforced layers respectively and can be calculated based on the Eshelby–Mori–Tanaka scheme as following [39, 40]:

$$K_{nc}=K_m+\frac{(\delta_r-3K_m\alpha_r)V_r}{3(V_m+V_r\alpha_r)}\quad G_{nc}=G_m+\frac{(\eta_r-2G_m\beta_r)V_r}{2(V_m+V_r\beta_r)} \tag{16}$$

in which G_m and K_m stand for shear and bulk moduli of the isotropic matrix which can be evaluated as

$$G_m=\frac{E_m}{2(1+\nu_m)},\quad K_m=\frac{E_m}{3(1-2\nu_m)}, \tag{17}$$

where E_m and ν_m are elasticity modulus and Poisson's ratio of the isotropic matrix and α_r, β_r, δ_r and η_r are defined as following [41]:

$$\begin{aligned}
\alpha_r&=\frac{3(K_m+G_m)+k_r+l_r}{3(G_m+k_r)},\\
\beta_r&=\frac{1}{5}\left[\frac{4G_m+2k_r+l_r}{3(G_m+k_r)}+\frac{4G_m}{G_m+p_r}+\frac{4G_m(3K_m+4G_m)}{G_m(3K_m+G_m)+m_r(3K_m+7G_m)}\right],\\
\delta_r&=\frac{1}{3}\left[n_r+2l_r+\frac{(2k_r+l_r)(3K_m+G_m-l_r)}{G_m+k_r}\right],\\
\eta_r&=\frac{1}{5}\left[\frac{2}{3}(n_r-l_r)+\frac{8G_mp_r}{G_m+p_r}+\frac{2(k_r-l_r)(2G_m+l_r)}{3(G_m+k_r)}+\frac{8m_rG_m(3K_m+4G_m)}{3K_m(G_m+m_r)+G_m(G_m+7m_r)}\right],
\end{aligned} \tag{18}$$

In Eq. (35), k_r, l_r, m_r, n_r and p_r are five independent constants known as Hill's elastic moduli [41].

2.4 Piezoelectric layers

For the piezoelectric face sheets, stress-strain relation can be written as follows [42]:

$$\begin{Bmatrix}\sigma_{xx}\\ \sigma_{yy}\\ \sigma_{zz}\\ \tau_{yz}\\ \tau_{xz}\\ \tau_{xy}\end{Bmatrix}=\begin{bmatrix}C_{11}&C_{12}&C_{13}&0&0&0\\ C_{12}&C_{22}&C_{13}&0&0&0\\ C_{13}&C_{13}&C_{33}&0&0&0\\ 0&0&0&C_{44}&0&0\\ 0&0&0&0&C_{55}&0\\ 0&0&0&0&0&C_{66}\end{bmatrix}\begin{Bmatrix}\varepsilon_{xx}\\ \varepsilon_{yy}\\ \varepsilon_{zz}\\ \gamma_{yz}\\ \gamma_{xz}\\ \gamma_{xy}\end{Bmatrix}-\begin{bmatrix}0&0&e_{31}\\ 0&0&e_{32}\\ 0&0&e_{33}\\ 0&e_{24}&0\\ e_{15}&0&0\\ 0&0&0\end{bmatrix}\begin{Bmatrix}E_x\\ E_y\\ E_z\end{Bmatrix} \tag{19-a}$$

$$\begin{Bmatrix} D_x \\ D_y \\ D_z \end{Bmatrix} = \begin{bmatrix} 0 & 0 & 0 & 0 & e_{15} & 0 \\ 0 & 0 & 0 & e_{24} & 0 & 0 \\ e_{31} & e_{32} & e_{33} & 0 & 0 & 0 \end{bmatrix} \begin{Bmatrix} \varepsilon_{xx} \\ \varepsilon_{yy} \\ \varepsilon_{zz} \\ \gamma_{yz} \\ \gamma_{xz} \\ \gamma_{xy} \end{Bmatrix} + \begin{bmatrix} k_{11} & 0 & 0 \\ 0 & k_{22} & 0 \\ 0 & 0 & k_{33} \end{bmatrix} \begin{Bmatrix} E_x \\ E_y \\ E_z \end{Bmatrix} \tag{19-b}$$

where C_{ij} are elastic coefficients of the piezoelectric layers, e_{ij} and k_{ij} are piezoelectric and dielectric coefficients, D is electric displacement and E_i show electric field which can be calculated using an electric potential function ($\Psi=\Psi(x,y,z,t)$) as

$$E_x = -\frac{\partial \Psi}{\partial x} \quad E_y = -\frac{\partial \Psi}{\partial y} \quad E_x = -\frac{\partial \Psi}{\partial z} \tag{20}$$

In this paper following distribution is considered for electric potential function [37].

$$\Psi(x,y,z,t) = \frac{2\psi_0}{h_p}\tilde{z} - \cos\left(\frac{\pi \tilde{z}}{h_p}\right)\psi(x,y,t) \tag{21}$$

in which ψ_0 is the electric potential implied on the top and bottom of the plate and $\psi= \psi(x,y,t)$ is an unspecified function and

$$\tilde{z} = \begin{cases} z_b = z + \dfrac{h_c}{2} + h_{nc} + \dfrac{h_p}{2} & \text{Bottom layer} \\ z_t = z - \dfrac{h_c}{2} - h_{nc} - \dfrac{h_p}{2} & \text{Top layer} \end{cases} \tag{22}$$

2.5 Hamilton's principle

The set of the governing equations can be derived using Hamilton's principle as [43]

$$\int_{t_1}^{t_2} \left(-\delta U + \delta T + \delta W_{n.c.}\right) dt = 0, \tag{23}$$

in which δ is a variational operator, $[t_1,t_2]$ is a desired time interval, U is strain energy, T is kinetic energy and $W_{n.c.}$ is work done by non-conservative forces.

The strain energy can be calculated as

$$U=\frac{1}{2}\iint_S\Bigg\{\int_{-\frac{h}{2}}^{-\frac{h_c}{2}-h_{nc}}\left[\sigma_{xx}\varepsilon_{xx}+\sigma_{yy}\varepsilon_{yy}+\sigma_{zz}\varepsilon_{zz}+\sigma_{xy}\gamma_{xy}+\sigma_{xz}\gamma_{xz}+\sigma_{yz}\gamma_{yz}-\left(D_xE_x+D_yE_y+D_zE_z\right)\right]dz+$$
$$\int_{-\frac{h_c}{2}-h_{nc}}^{-\frac{h_c}{2}}\left(\sigma_{xx}\varepsilon_{xx}+\sigma_{yy}\varepsilon_{yy}+\sigma_{zz}\varepsilon_{zz}+\sigma_{xy}\gamma_{xy}+\sigma_{xz}\gamma_{xz}+\sigma_{yz}\gamma_{yz}\right)dz+$$
$$\int_{-\frac{h_c}{2}}^{\frac{h_c}{2}}\left(\sigma_{xx}\varepsilon_{xx}+\sigma_{yy}\varepsilon_{yy}+\sigma_{zz}\varepsilon_{zz}+\sigma_{xy}\gamma_{xy}+\sigma_{xz}\gamma_{xz}+\sigma_{yz}\gamma_{yz}\right)dz+ \tag{24}$$
$$\int_{\frac{h_c}{2}}^{\frac{h_c}{2}+h_{nc}}\left(\sigma_{xx}\varepsilon_{xx}+\sigma_{yy}\varepsilon_{yy}+\sigma_{zz}\varepsilon_{zz}+\sigma_{xy}\gamma_{xy}+\sigma_{xz}\gamma_{xz}+\sigma_{yz}\gamma_{yz}\right)dz+$$
$$\int_{\frac{h_c}{2}+h_{cn}}^{\frac{h}{2}}\left[\sigma_{xx}\varepsilon_{xx}+\sigma_{yy}\varepsilon_{yy}+\sigma_{zz}\varepsilon_{zz}+\sigma_{xy}\gamma_{xy}+\sigma_{xz}\gamma_{xz}+\sigma_{yz}\gamma_{yz}-\left(D_xE_x+D_yE_y+D_zE_z\right)\right]dz\Bigg\}dS$$

in which S is the surface of the plate. The kinetic energy can be stated as

$$T=\frac{1}{2}\iint_S\Bigg\{\int_{-\frac{h}{2}}^{-\frac{h_c}{2}-h_{nc}}\rho_p\left[\left(\frac{\partial u_1}{\partial t}\right)^2+\left(\frac{\partial u_2}{\partial t}\right)^2+\left(\frac{\partial u_3}{\partial t}\right)^2\right]dz+\int_{-\frac{h_c}{2}-h_{nc}}^{-\frac{h_c}{2}}\rho_{nc}\left[\left(\frac{\partial u_1}{\partial t}\right)^2+\left(\frac{\partial u_2}{\partial t}\right)^2+\left(\frac{\partial u_3}{\partial t}\right)^2\right]dz+$$
$$\int_{-\frac{h_c}{2}}^{\frac{h_c}{2}}\rho_c\left[\left(\frac{\partial u_1}{\partial t}\right)^2+\left(\frac{\partial u_2}{\partial t}\right)^2+\left(\frac{\partial u_3}{\partial t}\right)^2\right]dz+\int_{\frac{h_c}{2}}^{\frac{h_c}{2}+h_{nc}}\rho_{nc}\left[\left(\frac{\partial u_1}{\partial t}\right)^2+\left(\frac{\partial u_2}{\partial t}\right)^2+\left(\frac{\partial u_3}{\partial t}\right)^2\right]dz+ \tag{25}$$
$$\int_{\frac{h_c}{2}+h_{cn}}^{\frac{h}{2}}\rho_p\left[\left(\frac{\partial u_1}{\partial t}\right)^2+\left(\frac{\partial u_2}{\partial t}\right)^2+\left(\frac{\partial u_3}{\partial t}\right)^2\right]dz\Bigg\}dS$$

The virtual work done by the external load can be stated as

$$\delta W_{ext}=\iint_S F\delta w dS \tag{26}$$

in which F is the load per unit area imposed by the foundation which can be stated based on the Pasternak model as follow:

$$F(x,y)=-K_w w+K_G\left(\frac{\partial^2 w}{\partial x^2}+\frac{\partial^2 w}{\partial y^2}\right) \tag{27}$$

where K_w and K_G are Winkler and shear coefficients of the foundation, respectively.

Substituting Eqs. (24)-(26) into Eq. (23) leads to the following governing equations:

$$\delta u : \frac{\partial N_{xx}}{\partial x}+\frac{\partial N_{xy}}{\partial y}-I_{11}\frac{\partial^2 u}{\partial t^2}-I_{13}\frac{\partial^2 \phi_x}{\partial t^2}+I_{12}\frac{\partial^3 w}{\partial x\,\partial t^2}=0$$

$$\delta v : \frac{\partial N_{yy}}{\partial y}+\frac{\partial N_{xy}}{\partial x}-I_{11}\frac{\partial^2 v}{\partial t^2}-I_{13}\frac{\partial^2 \phi_y}{\partial t^2}+I_{12}\frac{\partial^3 w}{\partial y\,\partial t^2}=0$$

$$\delta w : \frac{\partial^2 M_{xx}}{\partial x^2}+2\frac{\partial^2 M_{xy}}{\partial y\,\partial x}+\frac{\partial^2 M_{yy}}{\partial y^2}-I_{11}\frac{\partial^2 w}{\partial t^2}-J_{13}\frac{\partial^2 \varnothing_z}{\partial t^2}-I_{12}\left(\frac{\partial^3 u}{\partial x\,\partial t^2}+\frac{\partial^3 v}{\partial y\,\partial t^2}\right)$$
$$+I_{22}\left(\frac{\partial^4 w}{\partial x^2\partial t^2}+\frac{\partial^4 w}{\partial y^2\partial t^2}\right)-I_{23}\left(\frac{\partial^3 \phi_x}{\partial x\,\partial t^2}+\frac{\partial^3 \phi_y}{\partial y\,\partial t^2}\right)-K_w w+K_G\left(\frac{\partial^2 w}{\partial x^2}+\frac{\partial^2 w}{\partial y^2}\right)=0$$

$$\delta\phi_x : \frac{\partial Q_{xx}}{\partial x}+\frac{\partial P_{xy}}{\partial y}-P_{xz}-I_{13}\frac{\partial^2 u}{\partial t^2}-I_{33}\frac{\partial^2 \phi_x}{\partial t^2}+I_{23}\frac{\partial^3 w}{\partial x\,\partial t^2}=0 \tag{28}$$

$$\delta\phi_y : \frac{\partial Q_{yy}}{\partial y}+\frac{\partial P_{xy}}{\partial x}-P_{yz}-I_{13}\frac{\partial^2 v}{\partial t^2}-I_{33}\frac{\partial^2 \phi_y}{\partial t^2}+I_{23}\frac{\partial^3 w}{\partial y\,\partial t^2}=0$$

$$\delta\phi_z : \frac{\partial P_{yz}}{\partial y}+\frac{\partial P_{xz}}{\partial x}-Q_{zz}-J_{21}\frac{\partial^2 w}{\partial t^2}-J_{22}\frac{\partial^2 \phi_z}{\partial t^2}=0$$

$$\delta\psi : \frac{\partial \bar{D}_x}{\partial x}+\frac{\partial \bar{D}_y}{\partial y}+\bar{D}_z=0$$

in which I_{ij} and J_{ij} are defined in Appendix A and

$$\begin{Bmatrix} N_{ij} \\ M_{ij} \\ P_{ij} \end{Bmatrix}=\int_{-\frac{h}{2}}^{\frac{h}{2}}\sigma_{ij}\begin{Bmatrix} 1 \\ z \\ \dfrac{df}{dz} \end{Bmatrix}dz \quad i,j=x,y,z$$

$$Q_{ij}=\int_{-\frac{h}{2}}^{\frac{h}{2}}\sigma_{ij}f(z)\,dz \quad \bar{D}_i=\int_{-\frac{h}{2}}^{\frac{h}{2}}D_i\cos\left(\frac{\pi z}{h_p}\right)dz \quad i,j=x,y \tag{29}$$

$$Q_{zz}=\int_{-\frac{h}{2}}^{\frac{h}{2}}\sigma_{ij}\frac{d^2 f}{dz^2}dz \quad \bar{D}_z=\frac{h_p}{\pi}\int_{-\frac{h}{2}}^{\frac{h}{2}}D_i\sin\left(\frac{\pi z}{h_p}\right)dz$$

By substituting Eqs. (3), (4), (19), (20) and (21) into Eqs. (28) and (29), the set of the governing equations can be written as

$$\delta u : \varsigma_{31}\frac{\partial \psi}{\partial x}-B_{11}\frac{\partial^3 w}{\partial x^3}+F_{11}\frac{\partial^2 \phi_x}{\partial x^2}+F_{12}\frac{\partial^2 \phi_y}{\partial x\,\partial y}-B_{12}\frac{\partial^3 w}{\partial y^2\partial x}+A_{13}\frac{\partial \phi_z}{\partial x}+A_{11}\frac{\partial^2 u}{\partial x^2}+A_{12}\frac{\partial^2 v}{\partial x\,\partial y}$$
$$+F_{66}\frac{\partial^2 \phi_x}{\partial y^2}+F_{66}\frac{\partial^2 \phi_y}{\partial x\,\partial y}-B_{66}\frac{\partial^3 w}{\partial y^2\partial x}+A_{66}\frac{\partial^2 u}{\partial y^2}+A_{66}\frac{\partial^2 v}{\partial x\,\partial y}-I_{13}\frac{\partial^2 \phi_x}{\partial t^2}+I_{12}\frac{\partial^3 w}{\partial t^2\partial x}-I_{11}\frac{\partial^2 u}{\partial t^2}=0$$

$$\delta v : \varsigma_{32}\frac{\partial \psi}{\partial y}-B_{22}\frac{\partial^3 w}{\partial y^3}+F_{22}\frac{\partial^2 \phi_y}{\partial y^2}+F_{12}\frac{\partial^2 \phi_x}{\partial x\,\partial y}-B_{12}\frac{\partial^3 w}{\partial x^2\partial y}+A_{23}\frac{\partial \phi_z}{\partial y}+A_{22}\frac{\partial^2 u}{\partial y^2}+A_{12}\frac{\partial^2 u}{\partial x\,\partial y} \tag{30}$$
$$+F_{66}\frac{\partial^2 \phi_y}{\partial x^2}+F_{66}\frac{\partial^2 \phi_x}{\partial x\,\partial y}-B_{66}\frac{\partial^3 w}{\partial x^2\partial y}+A_{66}\frac{\partial^2 u}{\partial x^2}+A_{66}\frac{\partial^2 u}{\partial x\,\partial y}-I_{13}\frac{\partial^2 \phi_y}{\partial t^2}+I_{12}\frac{\partial^3 w}{\partial t^2\partial y}-I_{11}\frac{\partial^2 v}{\partial t^2}=0$$

$$\delta w : 2H_{66}\frac{\partial^3\phi_y}{\partial y\,\partial x^2}-2D_{66}\frac{\partial^4 w}{\partial y^2\partial x^2}+I_{22}\frac{\partial^4 w}{\partial x^2\partial t^2}-I_{12}\frac{\partial^3 v}{\partial t^2\partial y}+I_{22}\frac{\partial^4 w}{\partial y^2\partial t^2}-D_{11}\frac{\partial^4 w}{\partial x^4}+B_{13}\frac{\partial^2\phi_z}{\partial x^2}+\iota_{31}\frac{\partial^2\psi}{\partial x^2}$$
$$+2H_{66}\frac{\partial^3\phi_x}{\partial x\,\partial y^2}+B_{66}\frac{\partial^3 u}{\partial y^2\partial x}+B_{66}\frac{\partial^3 v}{\partial y\,\partial x^2}+H_{11}\frac{\partial^3\phi_x}{\partial x^3}+H_{12}\frac{\partial^3\phi_y}{\partial y\,\partial x^2}-2D_{12}\frac{\partial^4 w}{\partial x^2\partial y^2}+B_{11}\frac{\partial^3 u}{\partial x^3}+B_{12}\frac{\partial^3 v}{\partial y\,\partial x^2}$$
$$+\mu_{32}\frac{\partial^2\psi}{\partial y^2}+B_{23}\frac{\partial^2\phi_z}{\partial y^2}+B_{12}\frac{\partial^3 u}{\partial x\,\partial y^2}+B_{22}\frac{\partial^3 v}{\partial y^3}+H_{12}\frac{\partial^3\phi_x}{\partial x\,\partial y^2}-D_{22}\frac{\partial^4 w}{\partial y^4}+H_{22}\frac{\partial^3\phi_y}{\partial y^3}-I_{23}\frac{\partial^3\phi_x}{\partial t^2\partial x}$$
$$-K_w w+K_G\frac{\partial^2 w}{\partial x^2}+K_G\frac{\partial^2 w}{\partial y^2}-I_{11}\frac{\partial^2 w}{\partial t^2}-I_{23}\frac{\partial^3\phi_y}{\partial t^2\partial y}-J_{21}\frac{\partial^2\phi_z}{\partial t^2}-I_{12}\frac{\partial^3 u}{\partial t^2\partial x}=0$$

$$\delta\phi_x : \mu_{31}\frac{\partial\psi}{\partial x}-H_{11}\frac{\partial^3 w}{\partial x^3}+F_{66}\frac{\partial^2 v}{\partial y\,\partial x}+L_{11}\frac{\partial^2\phi_x}{\partial x^2}-H_{12}\frac{\partial^3 w}{\partial y^2\partial x}+F_{13}\frac{\partial\phi_z}{\partial x}+F_{66}\frac{\partial^2 u}{\partial y^2}+F_{12}\frac{\partial^2 v}{\partial x\,\partial y}+L_{66}\frac{\partial^2\phi_x}{\partial y^2}+L_{12}\frac{\partial^2}{\partial x}$$
$$-2H_{66}\frac{\partial^3 w}{\partial y^2\partial x}+L_{66}\frac{\partial^2\phi_y}{\partial x\,\partial y}+F_{11}\frac{\partial^2 u}{\partial x^2}-I_{13}\frac{\partial^2 u}{\partial t^2}+I_{23}\frac{\partial^3 w}{\partial t^2\partial x}-I_{33}\frac{\partial^2\phi_x}{\partial t^2}-L_{55}\frac{\partial\phi_z}{\partial x}+\tau_{15}\frac{\partial\psi}{\partial x}-L_{55}\phi_x=0$$
$$\delta\phi_y : \mu_{32}\frac{\partial\psi}{\partial y}-H_{22}\frac{\partial^3 w}{\partial y^3}+F_{66}\frac{\partial^2 u}{\partial y\,\partial x}+L_{22}\frac{\partial^2\phi_y}{\partial y^2}-H_{12}\frac{\partial^3 w}{\partial x^2\partial y}+F_{23}\frac{\partial\phi_z}{\partial y}+F_{66}\frac{\partial^2 v}{\partial x^2}+F_{12}\frac{\partial^2 u}{\partial x\,\partial y}+L_{66}\frac{\partial^2\phi_y}{\partial x^2}+F_{22}\frac{\partial}{\partial}$$
$$+L_{12}\frac{\partial^2\phi_x}{\partial x\,\partial y}-2H_{66}\frac{\partial^3 w}{\partial x^2\partial y}+L_{66}\frac{\partial^2\phi_x}{\partial x\,\partial y}-L_{44}\frac{\partial\phi_z}{\partial y}+\tau_{24}\frac{\partial\psi}{\partial y}-L_{44}\phi_y-I_{33}\frac{\partial^2\phi_y}{\partial t^2}-I_{13}\frac{\partial^2 v}{\partial t^2}+I_{23}\frac{\partial^3 w}{\partial t^2\partial y}=0$$
$$\delta\phi_z : -\tau_{15}\frac{\partial^2\psi}{\partial x^2}+L_{55}\frac{\partial\phi_x}{\partial x}+L_{55}\frac{\partial^2\phi_z}{\partial x^2}+B_{13}\frac{\partial^2 w}{\partial x^2}-F_{13}\frac{\partial\phi_x}{\partial x}+B_{23}\frac{\partial^2 w}{\partial y^2}-\tau_{24}\frac{\partial^2\psi}{\partial y^2}+L_{44}\frac{\partial^2\phi_z}{\partial y^2}+L_{44}\frac{\partial\phi_y}{\partial y}$$
$$+B_{13}\frac{\partial^2 w}{\partial x^2}-F_{13}\frac{\partial\phi_x}{\partial x}+B_{23}\frac{\partial^2 w}{\partial y^2}-A_{33}\phi_z-\varsigma_{33}\psi-F_{23}\frac{\partial\phi_y}{\partial y}-A_{13}\frac{\partial u}{\partial x}-A_{23}\frac{\partial v}{\partial y}-J_{21}\frac{\partial^2 w}{\partial t^2}-J_{22}\frac{\partial^2\phi_z}{\partial t^2}=0$$

$$\delta\psi : \tau_{15}\frac{\partial\phi_x}{\partial x}+\tau_{15}\frac{\partial^2\phi_z}{\partial x^2}+\Xi_{11}\frac{\partial^2\psi}{\partial x^2}+\tau_{24}\frac{\partial\phi_y}{\partial y}+\tau_{24}\frac{\partial^2\phi_z}{\partial y^2}+\Xi_{22}\frac{\partial^2\psi}{\partial y^2}-\Xi_{33}\psi+\mu_{31}\frac{\partial\phi_x}{\partial x}$$
$$+\mu_{32}\frac{\partial\phi_y}{\partial y}-\iota_{31}\frac{\partial^2 w}{\partial x^2}-\iota_{32}\frac{\partial^2 w}{\partial y^2}+\varsigma_{33}\phi_z+\varsigma_{31}\frac{\partial u}{\partial x}+\varsigma_{32}\frac{\partial v}{\partial y}=0$$

3 SOLUTION PROCEDURE

For a simply supported plate, the following solution can be considered based on Navier's solution:

$$
\begin{aligned}
u(x,y,t) &= \sum_{m=1}^{\infty}\sum_{n=1}^{\infty} U_{mn}\cos\left(\frac{m\pi}{a}x\right)\sin\left(\frac{n\pi}{b}y\right)e^{i\omega t}\\
v(x,y,t) &= \sum_{m=1}^{\infty}\sum_{n=1}^{\infty} V_{mn}\cos\left(\frac{m\pi}{a}x\right)\sin\left(\frac{n\pi}{b}y\right)e^{i\omega t}\\
w(x,y,t) &= \sum_{m=1}^{\infty}\sum_{n=1}^{\infty} W_{mn}\cos\left(\frac{m\pi}{a}x\right)\sin\left(\frac{n\pi}{b}y\right)e^{i\omega t}\\
\phi_x(x,y,t) &= \sum_{m=1}^{\infty}\sum_{n=1}^{\infty} X_{mn}\cos\left(\frac{m\pi}{a}x\right)\sin\left(\frac{n\pi}{b}y\right)e^{i\omega t}\\
\phi_y(x,y,t) &= \sum_{m=1}^{\infty}\sum_{n=1}^{\infty} Y_{mn}\cos\left(\frac{m\pi}{a}x\right)\sin\left(\frac{n\pi}{b}y\right)e^{i\omega t}\\
\phi_z(x,y,t) &= \sum_{m=1}^{\infty}\sum_{n=1}^{\infty} Z_{mn}\cos\left(\frac{m\pi}{a}x\right)\sin\left(\frac{n\pi}{b}y\right)e^{i\omega t}\\
\psi(x,y,t) &= \sum_{m=1}^{\infty}\sum_{n=1}^{\infty} \Psi_{mn}\cos\left(\frac{m\pi}{a}x\right)\sin\left(\frac{n\pi}{b}y\right)e^{i\omega t}
\end{aligned}
\tag{31}
$$

Substituting Eq. (31) into Eq. (30) leads to the following eigenvalue equation:

$$
[K]\begin{Bmatrix} U_{mn}\\ V_{mn}\\ W_{mn}\\ X_{mn}\\ Y_{mn}\\ Z_{mn}\\ \Psi_{mn}\end{Bmatrix} = \omega^2[M]\begin{Bmatrix} U_{mn}\\ V_{mn}\\ W_{mn}\\ X_{mn}\\ Y_{mn}\\ Z_{mn}\\ \Psi_{mn}\end{Bmatrix}
\tag{32}
$$

in which, [K] and [M] are stiffness and mass matrices, respectively. These two symmetric matrices are presented by details in Appendix C. By solving the eigenvalue equation (30), the natural frequencies of the 5-layer sandwich plate can be achieved for different values of mode numbers m and n.

4 NUMERICAL RESULTS

In this section, numerical results are reported for the analytical solution presented previously. For the sake of validation, consider a single layer homogeneous square plate of a/h=10 and ν=0.3 with no foundation (K_w=0, K_G=0). For different values of mode numbers m and n, dimensionless natural frequency of the plate ($\lambda=\omega h(\rho/G)^{0.5}$) are presented in Table 1 against corresponding ones reported by other authors [44, 45]. As shown in this table, results with high accuracy can be obtained.

Table 1
Dimensionless natural frequencies ($\lambda=\omega h(\rho/G)^{0.5}$) of a single layer, homogeneous square plate (a/h=10, ν=0.3, K_w=0, K_G=0)

(m,n)	Present	Exact 3D solution [44]	HSDT [45]
(1,1)	0.0933	0.0932	0.0931
(1,2)	0.2230	0.2226	0.2222
(2,2)	0.3428	0.3421	0.3411
(1,3)	0.4182	0.4171	0.4158
(2,3)	0.5253	0.5239	0.5221
(3,3)	0.6911	0.6889	0.6862
(2,4)	0.7537	0.7511	0.7481
(1,5)	0.9304	0.9268	0.9230
(4,4)	1.0938	1.0889	1.0847
Maximum Error (%)	-	0.45	0.83

Again, a single layer homogeneous rectangular plate of a/b=0.5, a/h=10 and ν=0.3 with no foundation (K_w=0, K_G=0) is selected. Table 2 shows dimensionless values of the natural frequency of the plate ($\Omega=\omega a^2(\rho/E)^{0.5}/h$) for various values of mode number m and n along with corresponding ones predicted by Hebali et al. [46]. As shown in this table, results are in high agreement.

Table 2
Dimensionless natural frequencies ($\Omega=\omega a^2(\rho/E)^{0.5}/h$) of a single layer homogeneous rectangular plate (a/b=0.5, a/h=10, ν=0.3, K_w=0, K_G=0)

(m,n)	Present	Quasi-3D [46]
(1,1)	3.70480	3.69590
(1,2)	5.85420	5.83920
(2,2)	13.9760	13.9324
(2,3)	17.1641	17.1070
(3,2)	26.1598	26.0579
(3,3)	28.9933	28.8754
Maximum Error (%)	-	0.79

Consider a thin square plate of b/h=300 and ν=0.3 with no foundation (K_w=0, K_G=0). Values of the first three natural frequencies are presented in Table 3 in a dimensionless form ($\Lambda=\omega a^2(\rho h/D)^{0.5}$, $D=Eh^3/12(1-\nu^2)$) against corresponding ones reported by other authors [15, 47-49]. This table confirms the high accuracy of the presented solution and the achieved results.

Table 3
Dimensionless natural frequencies ($\Lambda=\omega a^2(\rho h/D)^{0.5}$, $D=Eh^3/12(1-\nu^2)$) of a single layer, homogeneous square plate (b/h=300, ν=0.3, K_w=0, K_G=0)

	Mode 1	Mode 2	Mode 3	Maximum Error (%)
Present work	19.7899	49.4718	98.9337	-
Exact solution [47]	19.7392	49.3480	98.6960	0.25
Finite element method [48]	19.7392	49.3480	98.7162	0.25
Differential quadrature method [49]	19.7392	49.3453	98.6268	0.31
Galerkin method [15]	19.7362	49.3431	98.6765	0.27

An isotropic homogeneous single layer square plate of ν=0.3 resting on an elastic foundation is considered. For different values of thickness to length ratio (h/a) and dimensionless Winkler and shear coefficients of the foundation ($\hat{K}_w = K_w a^4/D$, $\hat{K}_G = K_G a^2/D$, $D=Eh^3/12(1-\nu^2)$), natural frequencies of the plate are presented in Table 4 in a dimensionless form ($\Lambda=\omega a^2(\rho h/D)^{0.5}$) against corresponding ones reported by other authors [50-52]. Results of this table confirm the accuracy of the presented solution.

Table 4
Dimensionless natural frequencies ($\Lambda=\omega a^2(\rho h/D)^{0.5}$, $D=Eh^3/12(1-\nu^2)$) of a single layer, homogeneous square plate (ν=0.3)

$\frac{h}{a}$	$\hat{K}_w, \hat{K}_G$	Akhavan et al. [50]	Atmane et al. [51]	Moradi et al. [52]	Present
0.001	(0,0)	19.7391	19.7392	19.7396	19.7904
	(100,10)	26.2112	26.2112	26.2115	26.2499
	(1000,100)	57.9961	57.9962	57.9963	58.0136
0.1	(0,0)	19.0840	19.0658	19.0658	19.1196
	(100,10)	25.6368	25.6236	25.6235	25.5733
	(1000,100)	57.3969	57.3923	57.3922	56.9680
0.2	(0,0)	17.5055	17.4531	17.4530	17.5141
	(100,10)	24.3074	24.2728	24.2728	23.9892
	(1000,100)	56.0359	56.0311	56.0363	56.0145

It what follows, numerical examples are presented to study the influences of various parameters on the natural frequencies of the 5-layer sandwich plates. Except for the cases which are mentioned directly, mechanical properties are considered as those mentioned in Table 5. Porosity distribution is considered as uneven with porosity parameter e_1=0.4 and CNTs are distributed with total volume fraction V^*_r=0.11 based on uniform distribution pattern. Elastic and shear stiffness coefficients of the foundation are selected as $K_w=10^{10}$ N/m^3 and $K_G=10^5$ N/m and the following dimensionless definition is defined for the natural frequencies:

$$\breve{\omega} = \omega h \sqrt{\frac{2(1+\nu)\rho_1}{E_1}} \tag{33}$$

Table 5
Mechanical properties

Core [37]	Interior layers		Piezoelectric face sheets [53]		
	Matrix[52]	CNT[14]			
			C_{11}=226 GPa		
		k_r=30 GPa	C_{12}=125 GPa		
		l_r=10 GPa	C_{13}=124 GPa		
E_1= 200 GPa	E=2.5 GPa	m_r=1 GPa	C_{22}=226 GPa	$e_{31}=e_{32}$=-2.2 C/m^2	$k_{11}=5.64\times10^{-9}$ C/Vm
ν=0.33	ν=0.34	n_r=450 GPa	C_{33}=216 GPa	$e_{15}=e_{24}$=5.8 C/m^2	$k_{22}=5.64\times10^{-9}$ C/Vm
ρ_1=7850 kg/m^3	ρ=1150 kg/m^3	p_r=1 GPa	C_{44}=44.2 GPa	e_{33}=9.3 C/m^2	$k_{33}=6.35\times10^{-9}$ C/Vm
		ρ_r=1400 kg/m^3	C_{55}=44.2 GPa		
			C_{66}=50.5 GPa		
			ρ=5550 kg/m^3		

For a sandwich plate of h_c/h_p=10 and h_p/h_{nc}=1 and constant surface area (S=ab), values of the natural frequencies are depicted versus aspect ratio (a/b) in Fig. 3. As shown in this figure, the minimum values of the natural belong to a square plate (a/b=1). For a/b<1 an increase in the value of aspect ratio decreases all natural frequencies and for a/b>1 reverse trend can be seen.

For a square sandwich plate, Fig. 4 shows the effect of thickness of the core to the thickness of the ratio of the CNT-reinforced layer (h_c/h_{nc}) on the values of the natural frequencies. As shown in this figure, with an increase in the value of h_c/h_{nc}, all natural frequencies reduce and get close to some constant values which are corresponding natural frequencies of a 3-layer sandwich plate with an FG porous core and piezoelectric face sheets.

For a sandwich plate of h_c/h_p=10 and h_p/h_{nc}=1, the effect of the porosity parameter and porosity distribution parameter on the values of the natural frequencies are illustrated in Figs. 5 and 6. As depicted in these figures all natural frequencies grow with an increase in porosity parameter which means that with an increase in the size of pores, the rate of the reduction in the inertia of the plate is higher than the reduction in stiffness. These figures also reveal that the value of the natural frequencies in even patterns is higher than the corresponding ones of the uneven pattern.

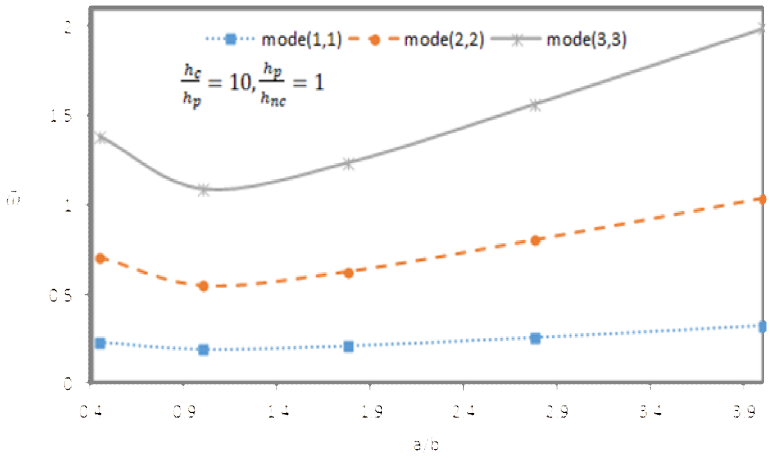

Fig. 3
Effect of aspect ratio (a/b) on the natural frequencies.

Error! Not a valid link.

Fig. 4
Effect of thickness of the core to the thickness of the ratio of the CNT-reinforced layer (h_c/h_{nc}) on the natural frequencies.

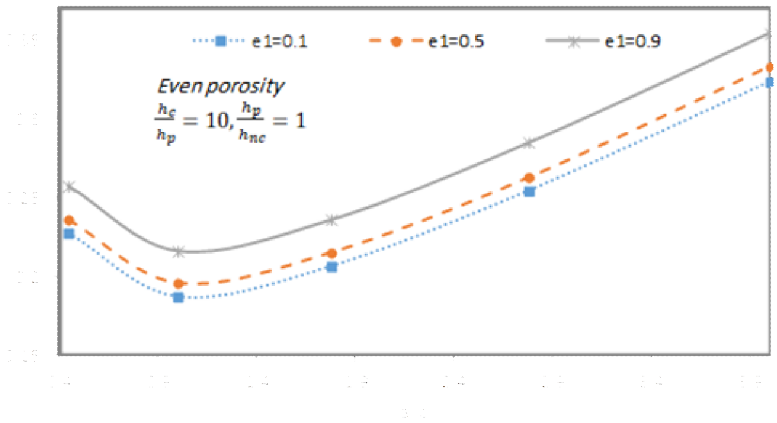

Fig. 5
Effect of porosity parameter on the natural frequencies for even pattern.

Fig. 7 shows the influence of the total volume fraction of CNTs on the natural frequencies of the sandwich plate of h_c/h_p=1 and h_p/h_{nc}=0.1. This figure confirms that all natural frequencies increase with the rise in the value of the total volume fraction of CNTs which can be explained by an increase in the flexural rigidity of the CNT-reinforced interior layers. In other words, as the volume fraction of CNTs in Eq. (16) becomes more, G_{nc} and K_{nc} that are shear and bulk moduli of the CNT-reinforced layers respectively, will increase. Therefore, according to Eq. (15), mechanical properties of nanocomposite layers increase. So the stiffness of the sandwich plate enhances which leads the natural frequency to increase. This result is in complete agreement with [11], [52] and [54].

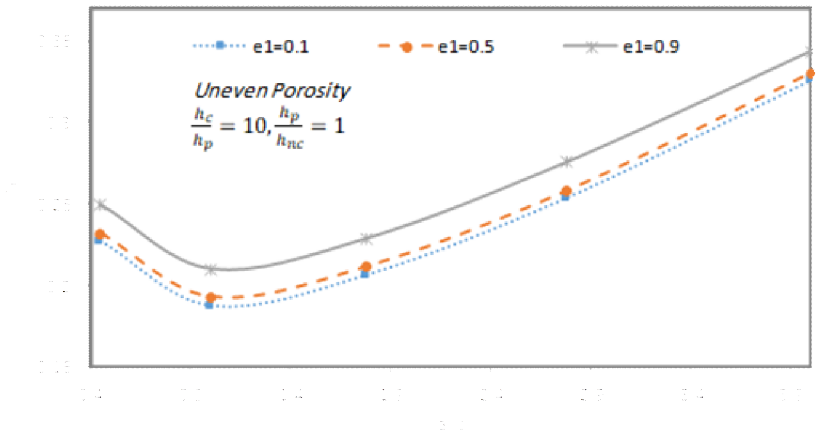

Fig. 6
Effect of porosity parameter on the natural frequencies for the uneven pattern.

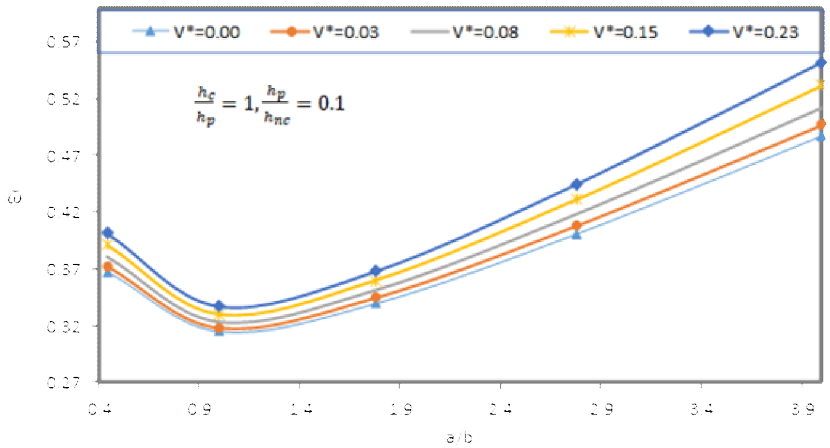

Fig. 7
Effect of volume fraction of CNTs on the natural frequencies.

For a sandwich square plate (a/b=1) of $h_c/h_p=1=h_p/h_{nc}=1$, Figs. 8 and 9 show the effect of Winkler and shear coefficients of the foundation on the natural frequencies. As these figures show, an increase in both Winkler and shear coefficients of the foundation, all natural frequencies grow which can be explained by the increase in the value of stiffness of the plate-foundation system.

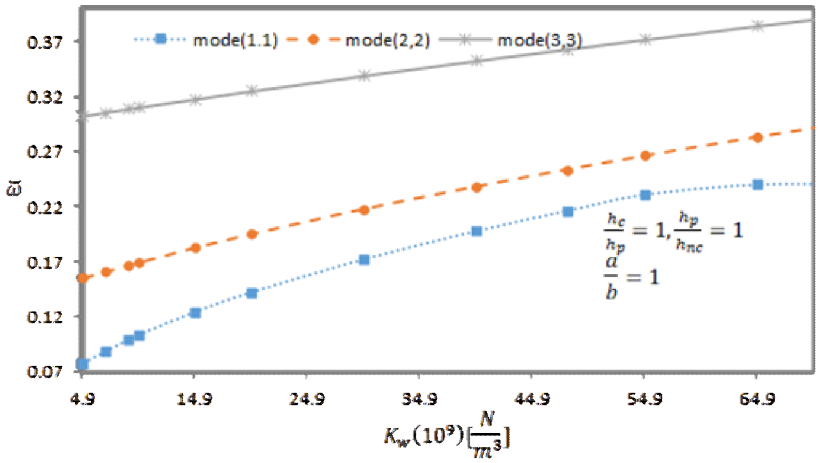

Fig. 8
Effect of Winkler coefficient of the foundation on the natural frequencies.

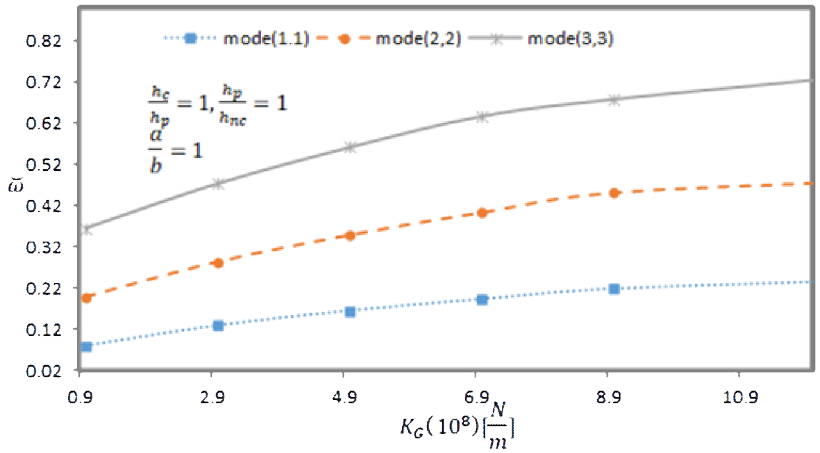

Fig. 9
Effect of shear coefficient of the foundation on the natural frequencies.

In order to study the effect of distribution patterns on CNTs on the natural frequencies, eight different couples of distribution patterns are considered as depicted in Fig. 10. For a sandwich plate of $h_c/h_p=1$ and $h_p/h_{nc}=0.1$, the variation of the fundamental frequency is depicted in Fig. 11 versus the aspect ratio for different couples of distribution patterns. As shown in this figure, the highest value of the fundamental frequency belongs to FG-VA and the lowest one belongs to FG-AV. In other words, in order to increase the reinforcing effect, it is better to put the CNTs as far as away from the middle surface (z=0).

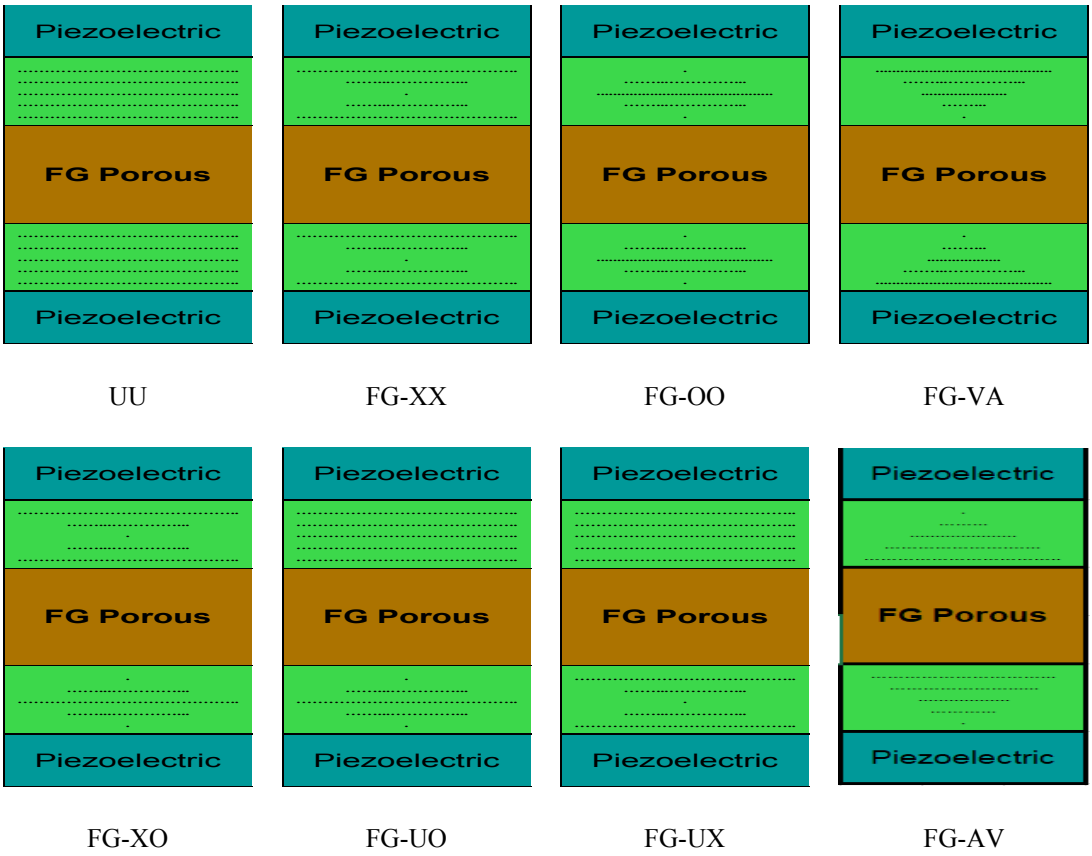

Fig. 10
Distribution patterns of CNTs.

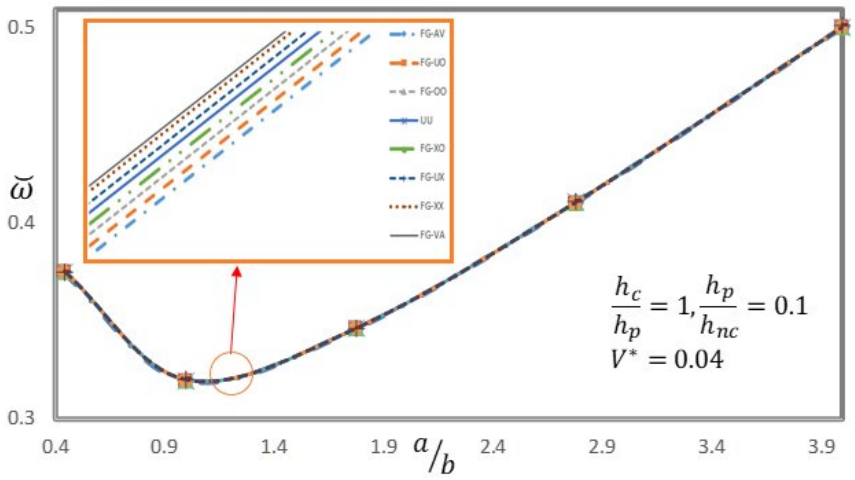

Fig. 11
Effect of distribution patterns of CNTs on the natural frequencies.

5 CONCLUSIONS

Using Navier's method, an exact solution was presented for free vibration characteristics of 5-layer sandwich plates consisted of an FGP core, CNT-reinforced interior layers and piezoelectric face sheets. The plate was modeled using the quasi-3D sinusoidal shear deformation theory and the set of the governing equations are derived using Hamilton's principle. The accuracy of the presented solution was validated and the influence of various parameters on the natural frequencies of the sandwich plate was investigated. It was concluded that by the assumption of constant surface area (S=ab), the minimum values of the natural belong to a square plate (a/b=1). Numerical examples showed that natural frequencies increase with the rise in the value of the porosity parameter (increase in the size of pores) and the even pattern for porosity distribution leads to higher values of natural frequencies rather than the uneven pattern. It was found that all natural frequencies increase with the rise in the value of the total volume fraction of CNTs and in order to maximize this increase, it is better to put the CNTs as far as away from the middle surface of the plate (z=0). It was concluded by numerical results that an increase in both Winkler and shear coefficients of the foundation leads to the increase in all natural frequencies of the plate.

APPENDIX A

$$\begin{aligned}\left\{I_{11},I_{12},I_{13},I_{22},I_{23},I_{33},J_{21},J_{22}\right\} = &\int_{-\frac{h}{2}}^{-\frac{h_c}{2}-h_{nc}} \rho_p \left\{1,z,f,z^2,zf,f^2,\frac{df}{dz},\left(\frac{df}{dz}\right)^2\right\}dz + \\ &\int_{-\frac{h_c}{2}-h_{nc}}^{-\frac{h_c}{2}} \rho_{nc} \left\{1,z,f,z^2,zf,f^2,\frac{df}{dz},\left(\frac{df}{dz}\right)^2\right\}dz + \int_{-\frac{h_c}{2}}^{\frac{h_c}{2}} \rho_c \left\{1,z,f,z^2,zf,f^2,\frac{df}{dz},\left(\frac{df}{dz}\right)^2\right\}dz + \\ &\int_{\frac{h_c}{2}}^{\frac{h_c}{2}+h_{nc}} \rho_{nc} \left\{1,z,f,z^2,zf,f^2,\frac{df}{dz},\left(\frac{df}{dz}\right)^2\right\}dz + \int_{\frac{h_c}{2}+h_{nc}}^{\frac{h}{2}} \rho_p \left\{1,z,f,z^2,zf,f^2,\frac{df}{dz},\left(\frac{df}{dz}\right)^2\right\}dz\end{aligned} \tag{A-1}$$

APPENDIX B

$$\left\{A_{ij},B_{ij},F_{ij},D_{ij},H_{ij},L_{ij}\right\}=\int_{-\frac{h}{2}}^{-\frac{h_c}{2}-h_{nc}}C_{ij}^{p}\left\{1,z,f,z^2,zf,f^2\right\}dz+\int_{-\frac{h_c}{2}-h_{nc}}^{-\frac{h_c}{2}}C_{ij}^{nc}\left\{1,z,f,z^2,zf,f^2\right\}dz+$$
$$\int_{-\frac{h_c}{2}}^{\frac{h_c}{2}}C_{ij}^{c}\left\{1,z,f,z^2,zf,f^2\right\}dz+\int_{\frac{h_c}{2}}^{\frac{h_c}{2}+h_{nc}}C_{ij}^{nc}\left\{1,z,f,z^2,zf,f^2\right\}dz+\int_{\frac{h_c}{2}+h_{nc}}^{\frac{h}{2}}C_{ij}^{p}\left\{1,z,f,z^2,zf,f^2\right\}dz$$
$$i,j=1,2$$

$$\left\{A_{ii},B_{ii},D_{ii},F_{ii},H_{ii},L_{ii}\right\}=\int_{-\frac{h}{2}}^{-\frac{h_c}{2}-h_{nc}}C_{44}^{p}\left\{1,z,z^2,\frac{df}{dz},z\frac{df}{dz},\left(\frac{df}{dz}\right)^2\right\}dz+$$
$$\int_{-\frac{h_c}{2}-h_{nc}}^{-\frac{h_c}{2}}C_{44}^{nc}\left\{1,z,z^2,\frac{df}{dz},z\frac{df}{dz},\left(\frac{df}{dz}\right)^2\right\}dz+\int_{-\frac{h_c}{2}}^{\frac{h_c}{2}}C_{44}^{c}\left\{1,z,z^2,\frac{df}{dz},z\frac{df}{dz},\left(\frac{df}{dz}\right)^2\right\}dz$$
$$+\int_{\frac{h_c}{2}}^{\frac{h_c}{2}+h_{nc}}C_{44}^{nc}\left\{1,z,z^2,\frac{df}{dz},z\frac{df}{dz},\left(\frac{df}{dz}\right)^2\right\}dz+\int_{\frac{h_c}{2}+h_{nc}}^{\frac{h}{2}}C_{44}^{p}\left\{1,z,z^2,\frac{df}{dz},z\frac{df}{dz},\left(\frac{df}{dz}\right)^2\right\}dz$$
$$i=4,5 \qquad \text{(B-1)}$$

$$\left\{A_{66},B_{66},D_{66},F_{66},H_{66},L_{66}\right\}=\int_{-\frac{h}{2}}^{-\frac{h_c}{2}-h_{nc}}C_{66}^{p}\left\{1,2z,2z^2,f,zf,f^2\right\}dz$$
$$\int_{-\frac{h_c}{2}-h_{nc}}^{-\frac{h_c}{2}}C_{66}^{nc}\left\{1,4z,4z^2,f,zf,f^2\right\}dz+\int_{-\frac{h_c}{2}}^{\frac{h_c}{2}}C_{66}^{c}\left\{1,2z,2z^2,f,zf,f^2\right\}dz+$$
$$\int_{\frac{h_c}{2}}^{\frac{h_c}{2}+h_{nc}}C_{66}^{nc}\left\{1,4z,4z^2,f,zf,f^2\right\}dz+\int_{\frac{h_c}{2}+h_{nc}}^{\frac{h}{2}}C_{66}^{p}\left\{1,2z,2z^2,f,zf,f^2\right\}dz$$

$$\left\{A_{i3},B_{i3},F_{i3}\right\}=\int_{-\frac{h}{2}}^{-\frac{h_c}{2}-h_{nc}}C_{i3}^{p}\left\{\frac{d^2f}{dz^2},z\frac{d^2f}{dz^2},f\frac{d^2f}{dz^2}\right\}dz+\int_{-\frac{h_c}{2}-h_{nc}}^{-\frac{h_c}{2}}C_{i3}^{nc}\left\{\frac{d^2f}{dz^2},z\frac{d^2f}{dz^2},f\frac{d^2f}{dz^2}\right\}dz+$$
$$\int_{-\frac{h_c}{2}}^{\frac{h_c}{2}}C_{i3}^{c}\left\{\frac{d^2f}{dz^2},z\frac{d^2f}{dz^2},f\frac{d^2f}{dz^2}\right\}dz+\int_{\frac{h_c}{2}}^{\frac{h_c}{2}+h_{nc}}C_{i3}^{nc}\left\{\frac{d^2f}{dz^2},z\frac{d^2f}{dz^2},f\frac{d^2f}{dz^2}\right\}dz+\int_{\frac{h_c}{2}+h_{nc}}^{\frac{h}{2}}C_{i3}^{p}\left\{\frac{d^2f}{dz^2},z\frac{d^2f}{dz^2},f\frac{d^2f}{dz^2}\right\}dz$$
$$i=1,2$$

$$A_{33} = \int_{-\frac{h}{2}}^{-\frac{h_c}{2}-h_{nc}} C_{33}^{p}\left(\frac{d^2 f}{dz^2}\right)^2 dz + \int_{-\frac{h_c}{2}-h_{nc}}^{-\frac{h_c}{2}} C_{33}^{nc}\left(\frac{d^2 f}{dz^2}\right)^2 dz +$$

$$\int_{-\frac{h_c}{2}}^{\frac{h_c}{2}} C_{33}^{c}\left(\frac{d^2 f}{dz^2}\right)^2 dz + \int_{\frac{h_c}{2}}^{\frac{h_c}{2}+h_{nc}} C_{33}^{nc}\left(\frac{d^2 f}{dz^2}\right)^2 dz + \int_{\frac{h_c}{2}+h_{nc}}^{\frac{h}{2}} C_{33}^{p}\left(\frac{d^2 f}{dz^2}\right)^2 dz$$

$$\left\{\varsigma_{3i}, \iota_{3i}, \mu_{3i}\right\} = \frac{\pi e_{3i}}{h_p}\left[\int_{-\frac{h}{2}}^{-\frac{h_c}{2}-h_{nc}} \sin\left(\frac{\pi z_b}{h_p}\right)\left\{1, z, f\right\} dz + \int_{\frac{h_c}{2}+h_{nc}}^{\frac{h}{2}} \sin\left(\frac{\pi z_t}{h_p}\right)\left\{1, z, f\right\} dz\right] \quad i = 1,2$$

$$\varsigma_{33} = \frac{\pi e_{33}}{h_p}\left[\int_{-\frac{h}{2}}^{-\frac{h_c}{2}-h_{nc}} \sin\left(\frac{\pi z_b}{h_p}\right)\frac{d^2 f}{dz^2} dz + \int_{\frac{h_c}{2}+h_{nc}}^{\frac{h}{2}} \sin\left(\frac{\pi z_t}{h_p}\right)\frac{d^2 f}{dz^2} dz\right]$$

$$\tau_{ij} = e_{ij}\left[\int_{-\frac{h}{2}}^{-\frac{h_c}{2}-h_{nc}} \frac{df}{dz}\cos\left(\frac{\pi z_b}{h_p}\right) dz + \int_{\frac{h_c}{2}+h_{nc}}^{\frac{h}{2}} \frac{df}{dz}\cos\left(\frac{\pi z_t}{h_p}\right) dz\right] \quad ij = 15,24$$

$$\Xi_{ii} = k_{ii}\left[\int_{-\frac{h}{2}}^{-\frac{h_c}{2}-h_{nc}} \cos^2\left(\frac{\pi z_b}{h_p}\right) dz + \int_{\frac{h_c}{2}+h_{nc}}^{\frac{h}{2}} \cos^2\left(\frac{\pi z_t}{h_p}\right) dz\right] \quad i = 1,2$$

$$\Xi_{33} = k_{33}\left(\frac{\pi}{h_p}\right)^2\left[\int_{-\frac{h}{2}}^{-\frac{h_c}{2}-h_{nc}} \sin^2\left(\frac{\pi z_t}{h_p}\right) dz + \int_{\frac{h_c}{2}+h_{nc}}^{\frac{h}{2}} \sin^2\left(\frac{\pi z_b}{h_p}\right) dz\right]$$

APPENDIX C

$$
\begin{aligned}
&K_{11}=-A_{11}\beta_1^2-A_{66}\beta_2^2 \quad K_{12}=-\beta_1\beta_2\left(A_{12}+A_{66}\right) \quad K_{13}=B_{11}\beta_1^3+\beta_1\beta_2^2\left(B_{12}+B_{66}\right)\\
&K_{14}=-F_{11}\beta_1^2-F_{66}\beta_2^2 \quad K_{15}=-\beta_1\beta_2\left(F_{12}+F_{66}\right) \quad K_{16}=A_{13}\beta_1\\
&K_{17}=\beta_1\varsigma_{31} \quad K_{22}=-A_{66}\beta_1^2-A_{22}\beta_2^2 \quad K_{23}=B_{22}\beta_2^3+\beta_2\beta_1^2\left(B_{12}+B_{66}\right)\\
&K_{24}=-\beta_1\beta_2\left(F_{12}+F_{66}\right) \quad K_{25}=-F_{66}\beta_1^2-F_{22}\beta_2^2 \quad K_{26}=\beta_2 A_{23}\\
&K_{27}=\beta_2\varsigma_{32} \quad K_{33}=-2\beta_1^2\beta_2^2\left(D_{66}+D_{12}\right)-\beta_1^4 D_{11}-\beta_2^4 D_{22}-K_W-K_G\left(\beta_1^2+\beta_2^2\right)\\
&K_{34}=H_{11}\beta_1^3+\beta_1\beta_2^2\left(H_{12}+2H_{66}\right) \quad K_{35}=H_{22}\beta_2^3+\beta_2\beta_1^2\left(H_{12}+2H_{66}\right) \quad K_{36}=-B_{13}\beta_1^2-B_{23}\beta_2^2\\
&K_{37}=-\beta_1^2\iota_{31}-\beta_2^2\iota_{32} \quad K_{44}=-L_{11}\beta_1^2-L_{66}\beta_2^2-L_{55} \quad K_{45}=-\beta_1\beta_2\left(L_{66}+L_{12}\right)\\
&K_{46}=\beta_1(F_{13}-L_{55}) \quad K_{47}=\beta_1\left(\mu_{31}+\tau_{15}\right) \quad K_{55}=-L_{22}\beta_2^2-L_{66}\beta_1^2-L_{44}\\
&K_{56}=\beta_2(F_{23}-L_{44}) \quad K_{57}=\beta_2\left(\mu_{32}+\tau_{24}\right) \quad K_{66}=-L_{44}\beta_2^2-L_{55}\beta_1^2-A_{33}\\
&K_{67}=\beta_1^2\tau_{15}+\beta_2^2\tau_{24}-\varsigma_{33} \quad K_{77}=\Xi_{11}\beta_1^2+\Xi_{22}\beta_2^2+\Xi_{33}
\end{aligned}
\tag{C-1}
$$

$$
M=\begin{bmatrix}
-I_{11} & 0 & \beta_1 I_{12} & -I_{13} & 0 & 0 & 0\\
 & -I_{11} & I_{12}\beta_2 & 0 & -I_{13} & 0 & 0\\
 & & -I_{11}-I_{22}\left(\beta_1^2+\beta_2^2\right) & I_{23}\beta_1 & I_{23}\beta_2 & -J_{21}\omega^2 & 0\\
 & & & -I_{33} & 0 & 0 & 0\\
 & & \textit{symmetric} & & -I_{33} & 0 & 0\\
 & & & & & -J_{22} & 0\\
 & & & & & & 0
\end{bmatrix}
$$

where

$$
\beta_1=\frac{m\pi}{a} \quad \beta_2=\frac{n\pi}{b} \tag{C-2}
$$

REFERENCES

[1] Chen, D., Yang, J. and Kitipornchai, S., 2015. Elastic buckling and static bending of shear deformable functionally graded porous beam. *Composite Structures*, *133*, pp.54-61.

[2] Chen, D., Yang, J. and Kitipornchai, S., 2016. Free and forced vibrations of shear deformable functionally graded porous beams. *International journal of mechanical sciences*, *108*, pp.14-22.

[3] Chen, D., Kitipornchai, S. and Yang, J., 2016. Nonlinear free vibration of shear deformable sandwich beam with a functionally graded porous core. *Thin-Walled Structures*, *107*, pp.39-48..

[4] Shafiei, N., Mousavi, A. and Ghadiri, M., 2016. On size-dependent nonlinear vibration of porous and imperfect functionally graded tapered microbeams. *International Journal of Engineering Science*, *106*, pp.42-56.

[5] Ebrahimi, F. and Jafari, A., 2016. Thermo-mechanical vibration analysis of temperature-dependent porous FG beams based on Timoshenko beam theory. *Struct. Eng. Mech*, *59*(2), pp.343-371.

[6] Barati, M.R. and Zenkour, A.M., 2018. Electro-thermoelastic vibration of plates made of porous functionally graded piezoelectric materials under various boundary conditions. *Journal of Vibration and Control*, *24*(10), pp.1910-1926.

[7] Ebrahimi, F. and Barati, M.R., 2017. Porosity-dependent vibration analysis of piezo-magnetically actuated heterogeneous nanobeams. *Mechanical Systems and Signal Processing*, *93*, pp.445-459.

[8] Safarpour, H., Mohammadi, K., Ghadiri, M. and Barooti, M.M., 2018. Effect of porosity on flexural vibration of CNT-reinforced cylindrical shells in thermal environment using GDQM. *International Journal of Structural Stability and Dynamics*, *18*(10), p.1850123.

[9] Shahsavari, D., Shahsavari, M., Li, L. and Karami, B., 2018. A novel quasi-3D hyperbolic theory for free vibration of FG plates with porosities resting on Winkler/Pasternak/Kerr foundation. *Aerospace Science and Technology*, *72*, pp.134-149.
[10] Daikh, A.A. and Zenkour, A.M., 2019. Effect of porosity on the bending analysis of various functionally graded sandwich plates. *Materials Research Express*, *6*(6), p.065703.
[11] Amir, S., Arshid, E., Rasti-Alhosseini, S.A. and Loghman, A., 2020. Quasi-3D tangential shear deformation theory for size-dependent free vibration analysis of three-layered FG porous micro rectangular plate integrated by nano-composite faces in hygrothermal environment. *Journal of Thermal Stresses*, *43*(2), pp.133-156
[12] Akbari, H., Azadi, M. and Fahham, H., 2020. Free vibration analysis of thick sandwich cylindrical panels with saturated FG-porous core. *Mechanics Based Design of Structures and Machines*, pp.1-19.
[13] Iijima, S., 1991. Helical microtubules of graphitic carbon. *nature*, *354*(6348), pp.56-58.
[14] Ghorbanpour Arani, A., Maghamikia, S., Mohammadimehr, M. and Arefmanesh, A., 2011. Buckling analysis of laminated composite rectangular plates reinforced by SWCNTs using analytical and finite element methods. *Journal of mechanical science and technology*, *25*(3), pp.809-820.
[15] Wang, Z.X. and Shen, H.S., 2012. Nonlinear vibration and bending of sandwich plates with nanotube-reinforced composite face sheets. *Composites Part B: Engineering*, *43*(2), pp.411-421.
[16] Zhu, P., Lei, Z.X. and Liew, K.M., 2012. Static and free vibration analyses of carbon nanotube-reinforced composite plates using finite element method with first order shear deformation plate theory. *Composite Structures*, *94*(4), pp.1450-1460.
[17] Lei, Z.X., Liew, K.M. and Yu, J.L., 2013. Buckling analysis of functionally graded carbon nanotube-reinforced composite plates using the element-free kp-Ritz method. *Composite Structures*, *98*, pp.160-168.
[18] Lei, Z.X., Liew, K.M. and Yu, J.L., 2013. Free vibration analysis of functionally graded carbon nanotube-reinforced composite plates using the element-free kp-Ritz method in thermal environment. *Composite Structures*, *106*, pp.128-138.
[19] Bhardwaj, G., Upadhyay, A.K., Pandey, R. and Shukla, K.K., 2013. Non-linear flexural and dynamic response of CNT reinforced laminated composite plates. *Composites Part B: Engineering*, *45*(1), pp.89-100.
[20] Alibeigloo, A., 2013. Static analysis of functionally graded carbon nanotube-reinforced composite plate embedded in piezoelectric layers by using theory of elasticity. *Composite Structures*, *95*, pp.612-622.
[21] Jeyaraj, P. and Rajkumar, I., 2013. Static behavior of FG-CNT polymer nano composite plate under elevated non-uniform temperature fields. *Procedia Engineering*, *64*, pp.825-834.
[22] Natarajan, S., Haboussi, M. and Manickam, G., 2014. Application of higher-order structural theory to bending and free vibration analysis of sandwich plates with CNT reinforced composite facesheets. *Composite Structures*, *113*, pp.197-207.
[23] Wattanasakulpong, N. and Chaikittiratana, A., 2015. Exact solutions for static and dynamic analyses of carbon nanotube-reinforced composite plates with Pasternak elastic foundation. *Applied Mathematical Modelling*, *39*(18), pp.5459-5472.
[24] Mohammadimehr, M., Monajemi, A.A. and Afshari, H., 2017. Free and forced vibration analysis of viscoelastic damped FG-CNT reinforced micro composite beams. *Microsystem Technologies*, pp.1-15..
[25] Mohammadimehr, M., Akhavan Alavi, S.M., Okhravi, S.V. and Edjtahed, S.H., 2018. Free vibration analysis of micro-magneto-electro-elastic cylindrical sandwich panel considering functionally graded carbon nanotube–reinforced nanocomposite face sheets, various circuit boundary conditions, and temperature-dependent material properties using high-order sandwich panel theory and modified strain gradient theory. *Journal of Intelligent Material Systems and Structures*, *29*(5), pp.863-882.
[26] Ghorbanpour Arani, A., Kiani, F. and Afshari, H., 2019. Aeroelastic analysis of laminated FG-CNTRC cylindrical panels under yawed supersonic flow. *International Journal of Applied Mechanics*, *11*(06), p.1950052.
[27] Ghorbanpour Arani, A., Kiani, F. and Afshari, H., 2019. Free and forced vibration analysis of laminated functionally graded CNT-reinforced composite cylindrical panels. *Journal of Sandwich Structures & Materials*, p.1099636219830787.
[28] Arefi, M., Kiani, M. and Zenkour, A.M., 2020. Size-dependent free vibration analysis of a three-layered exponentially graded nano-/micro-plate with piezomagnetic face sheets resting on Pasternak's foundation via MCST. *Journal of Sandwich Structures & Materials*, *22*(1), pp.55-86.
[29] Zenkour, A.M., 2005. On vibration of functionally graded plates according to a refined trigonometric plate theory. *International Journal of Structural Stability and Dynamics*, *5*(02), pp.279-297.
[30] Zenkour, A.M., 2007. Benchmark trigonometric and 3-D elasticity solutions for an exponentially graded thick rectangular plate. *Archive of Applied Mechanics*, *77*(4), pp.197-214.
[31] Levy, M., 1877. Mémoire sur la théorie des plaques élastiques planes. *Journal de mathématiques pures et appliquées*, pp.219-306.
[32] Stein, M., 1986. Nonlinear theory for plates and shells including the effects of transverse shearing. *AIAA journal*, *24*(9), pp.1537-1544.
[33] Zenkour, A.M., Allam, M.N.M., Radwan, A.F. and El-Mekawy, H.F., 2015. Thermo-mechanical bending response of exponentially graded thick plates resting on elastic foundations. *International Journal of Applied Mechanics*, *7*(04), p.1550062.
[34] Zenkour, A.M., 2013. Bending analysis of functionally graded sandwich plates using a simple four-unknown shear and normal deformations theory. *Journal of Sandwich Structures & Materials*, *15*(6), pp.629-656.
[35] Sadd, M.H., 2009. *Elasticity: theory, applications, and numerics*. Academic Press.
[36] Reddy, J.N., 2003. *Mechanics of laminated composite plates and shells: theory and analysis*. CRC press.

[37] Ghorbanpour Arani, A. and Zamani, M.H., 2019. Investigation of electric field effect on size-dependent bending analysis of functionally graded porous shear and normal deformable sandwich nanoplate on silica Aerogel foundation. *Journal of Sandwich Structures & Materials*, *21*(8), pp.2700-2734.
[38] Moradi-Dastjerdi, R. and Behdinan, K., 2020. Stability analysis of multifunctional smart sandwich plates with graphene nanocomposite and porous layers. *International Journal of Mechanical Sciences*, *167*, p.105283.
[39] Eshelby, J.D., 1957. The determination of the elastic field of an ellipsoidal inclusion, and related problems. *Proceedings of the royal society of London. Series A. Mathematical and physical sciences*, *241*(1226), pp.376-396.
[40] Mori, T. and Tanaka, K., 1973. Average stress in matrix and average elastic energy of materials with misfitting inclusions. *Acta metallurgica*, *21*(5), pp.571-574.
[41] Hill, R., 1965. A self-consistent mechanics of composite materials. *Journal of the Mechanics and Physics of Solids*, *13*(4), pp.213-222.
[42] Ghorbanpour Arani, A., Khani Arani, H. and Khoddami Maraghi, Z., 2016. Vibration analysis of sandwich composite micro-plate under electro-magneto-mechanical loadings. *Applied Mathematical Modelling*, *40*(23-24), pp.10596-10615.
[43] J.N. Reddy, Energy principles and variational methods in applied mechanics, John Wiley & Sons2017.
[44] Srinivas, S., Rao, C.J. and Rao, A.K., 1970. An exact analysis for vibration of simply-supported homogeneous and laminated thick rectangular plates. *Journal of sound and vibration*, *12*(2), pp.187-199.
[45] Reddy, J.N. and Phan, N.D., 1985. Stability and vibration of isotropic, orthotropic and laminated plates according to a higher-order shear deformation theory. *Journal of sound and vibration*, *98*(2), pp.157-170.
[46] Hebali, H., Tounsi, A., Houari, M.S.A., Bessaim, A. and Bedia, E.A.A., 2014. New quasi-3D hyperbolic shear deformation theory for the static and free vibration analysis of functionally graded plates. *Journal of Engineering Mechanics*, *140*(2), pp.374-383.
[47] Leissa, A.W., 1973. The free vibration of rectangular plates. *Journal of sound and vibration*, *31*(3), pp.257-293.
[48] Bardell, N.S., 1989. The application of symbolic computing to the hierarchical finite element method. *International Journal for Numerical Methods in Engineering*, *28*(5), pp.1181-1204.
[49] X. Wang, Y.L. Wang, R.B. Chen, Static and free vibrational analysis of rectangular plates by the differential quadrature element method, Communications in Numerical Methods in Engineering 14(12) (1998) 1133-1141.
[50] Akhavan, H., Hashemi, S.H., Taher, H.R.D., Alibeigloo, A. and Vahabi, S., 2009. Exact solutions for rectangular Mindlin plates under in-plane loads resting on Pasternak elastic foundation. Part II: Frequency analysis. *Computational Materials Science*, *44*(3), pp.951-961.
[51] Atmane, H.A., Tounsi, A. and Mechab, I., 2010. Free vibration analysis of functionally graded plates resting on Winkler–Pasternak elastic foundations using a new shear deformation theory. *International Journal of Mechanics and Materials in Design*, *6*(2), pp.113-121.
[52] Moradi-Dastjerdi, R., Payganeh, G. and Malek-Mohammadi, H., 2015. Free vibration analyses of functionally graded CNT reinforced nanocomposite sandwich plates resting on elastic foundation. *Journal of Solid Mechanics*, *7*(2), pp.158-172.
[53] Arefi, M., Zamani, M.H. and Kiani, M., 2018. Size-dependent free vibration analysis of three-layered exponentially graded nanoplate with piezomagnetic face-sheets resting on Pasternak's foundation. Journal of Intelligent Material Systems and Structures, 29(5), pp.774-786.
[54] Ghorbanpour Arani, A., BabaAkbar Zarei, H. and Haghparast, E., 2018. Vibration response of viscoelastic sandwich plate with magnetorheological fluid core and functionally graded-piezoelectric nanocomposite face sheets. *Journal of Vibration and Control*, *24*(21), pp.5169-5185.